PHYSICAL REVIEW B **82**, 161416(R) (2010)

Electron-avalanche amplifier based on the electronic Venturi effect

D. Taubert,[1] G. J. Schinner,[1] H. P. Tranitz,[2] W. Wegscheider,[3] C. Tomaras,[1] S. Kehrein,[1] and S. Ludwig[1]
[1]*Center for NanoScience and Fakultät für Physik, Ludwig-Maximilians-Universität, Geschwister-Scholl-Platz 1, 80539 München, Germany*
[2]*Institut für Experimentelle Physik, Universität Regensburg, 93040 Regensburg, Germany*
[3]*Solid State Physics Laboratory, ETH Zurich, 8093 Zurich, Switzerland*
(Received 5 October 2010; published 21 October 2010)

Scattering of otherwise ballistic electrons far from equilibrium is investigated in a cold two-dimensional electron system. The interaction between excited electrons and the degenerate Fermi liquid induces a positive charge in a nanoscale region which would be negatively charged for diffusive transport at local thermal equilibrium. In a three-terminal device we observe avalanche amplification of electrical current, resulting in a situation comparable to the Venturi effect in hydrodynamics. Numerical calculations using a random-phase approximation are in agreement with our data and suggest Coulomb interaction as the dominant scattering mechanism.

DOI: 10.1103/PhysRevB.82.161416 PACS number(s): 73.23.−b, 67.10.Jn, 73.50.Gr

Bernoulli's principle states that an increase in velocity of an inviscid fluid is accompanied by a pressure decrease. A related "hydrodynamic" effect on the nanoscale has been predicted by Govorov *et al.*[1] who consider a degenerate high-mobility Fermi liquid instead of a classical inviscid fluid. *Hot* electrons are injected through a quantum point contact (QPC) and then move ballistically along a two-dimensional electron system (2DES). They transfer energy and forward momentum to electrons from the degenerate Fermi sea which causes a net positive charge to be left behind. This effect, based on momentum transfer, has so far eluded experimental proof. In classical hydrodynamics Bernoulli's principle combined with the continuity equation leads to the Venturi effect. That is, the pressure in a fluid decreases as it passes through a tube with reduced cross section. In a spectacular application, the water jet pump introduced by Bunsen in 1869,[2] the reduced pressure is utilized for evacuating a side port. After passing the side port the fluid is decelerated into a wider collector tube which also seals the pump from its exhaust and improves the vacuum. Here we present a nanoscale device which behaves similarly to a water jet pump, "pumping" electrons instead of a classical fluid. Our electron jet pump follows the idea described in Ref. 1 but is enhanced by an additional barrier "BC" that separates the side contact from the collector [see Fig. 1(a); electrons are injected from the left]. Excited electrons which carry enough forward momentum can pass BC and reach the collector contact "C" but positively charged holes (in the Fermi sea) are reflected. If the side contact is grounded, the positive charge is neutralized by electrons flowing from the side into the device. This flow adds to the electron current from the emitter to create an amplified current at the collector port. Our electron jet pump is therefore a prototype of a ballistic electron-avalanche amplifier. We observe amplification up to a factor of seven which hints at several electron-electron scattering events per electron between emitter (QPC) and collector.

Amplifiers based on the injection of hot electrons have been pursued since the 1980s in various transistor structures[3–5] and high-mobility 2DESs.[6–8] Our systematic investigations go well beyond those previous publications and give the perspective of a detailed understanding of nonequilibrium transport in Fermi liquids. While this also includes the emission of acoustic[9] and optical[7,10] phonons and plasmons, here we focus on scattering between electrons (see, e.g., Ref. 11, which considers much lower energies than covered here). In our experiments we realize a transition from a regime in which the electron-electron scattering length l_{ee} is small compared to the sample dimensions (avalanche amplification) to purely ballistic motion of hot electrons. Our avalanche amplifier also promises future applications, e.g., as a new kind of charge detector.

The device shown in Fig. 1(a) has been fabricated from a GaAs/AlGaAs heterostructure which contains a 2DES 90 nm below the surface. The sample consists of a hallbar with several ohmic contacts (not visible). Three terminals are used as emitter "E," "side" contact, and collector C. Metallic gates

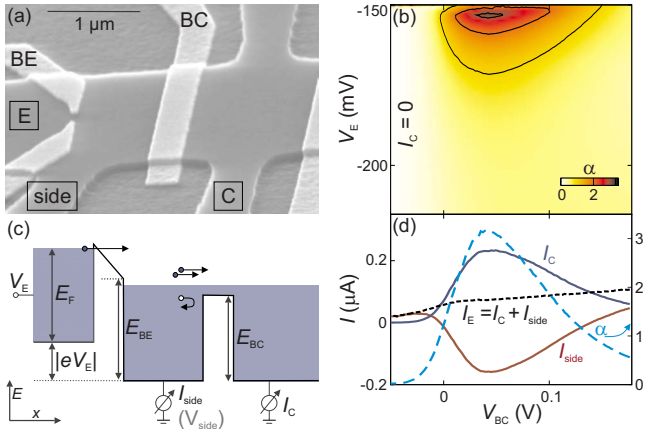

FIG. 1. (Color online) (a) Electron micrograph of the hallbar (elevated area), fabricated by wet etching, which contains the 2DES. Top gates (light gray) are used to define electrostatic barriers BE and BC. Ohmic contacts E, side, and C are marked. (b) Transfer ratio $\alpha = I_C/I_E$, plotted against barrier voltage V_{BC} and bias V_E ($V_{BE} = -0.925$ V). Contour lines show $\alpha = 1, 2, 3$. (c) Energy diagram sketching the experiment. (d) Relevant currents as well as transfer ratio along a horizontal cross-section of Fig. 1(b) at $V_E = -153$ mV.

(light gray) serve to define a broad collector barrier BC and an emitter QPC "BE" electrostatically. The use of a QPC as emitter is not crucial; very similar data have been taken with a broad emitter barrier instead. As sketched in Fig. 1(c), electrons are injected from the emitter E at potential $V_E<0$ into the region between BE and BC. By tuning BE near pinch-off, it is assured that the injected electrons have a kinetic energy close to $|eV_E|+E_F$ (E_F is the Fermi energy). At first these hot electrons move ballistically toward BC. Eventually they scatter and excite additional electrons from the degenerate Fermi sea, thereby transferring part of their energy and momentum. Conduction-band holes in the Fermi sea are left behind [Fig. 1(c)]. The collector barrier separates excited electrons (which can pass the barrier) from the holes (which are reflected); the accumulation of holes causes a buildup of positive charge between BE and BC. The measured currents I_C and I_{side} are defined to be positive when electrons flow from the sample *into* the respective terminals, as would be expected in diffusive transport. Here, we tune our devices away from the diffusive-transport regime. In contrast to many previous publications[3–5] we reach a ballistic regime which is far from local thermal equilibrium.

The mobility and Fermi energy of the 2DES are $\mu=1.4\times10^6$ cm^2/(V s) (at $T\approx1$ K) and $E_F=9.7$ meV (carrier density $n_s=2.7\times10^{15}$ m^{-2}). In our case the elastic mean-free path $l_m\simeq12$ μm exceeds the dimensions of the nanostructure by far. Measurements shown here have been performed in a ^{3}He cryostat at $T_{bath}\simeq260$ mK but comparable results have been obtained in a wide temperature range of 20 mK$\leq T_{bath}\leq$20 K in similar samples.

To probe for amplification, we consider the transfer ratio $\alpha=I_C/I_E$ with $I_E\equiv I_C+I_{side}$ the current injected from E. As a typical example α is plotted in Fig. 1(b) as a function of V_E and V_{BC}. Amplification ($\alpha>1$) is observed in a limited region which is framed by contour lines. We have already reached $\alpha\simeq7$ in a similar setup (here $\alpha\lesssim3.2$). The actually measured currents I_C and I_{side} are shown in Fig. 1(d) for constant $V_E=-153$ mV. For very negative V_{BC}, the collector barrier BC is closed, $I_{side}=I_E$, and $\alpha=0=I_C$. As BC is opened, I_C shows a broad maximum, exceeding I_E. Hence, electrons are drawn in from the side contact ($I_{side}<0, \alpha>1$), making the device an electron jet pump. In the limit of a wide-open collector barrier (large V_{BC}) the electron-hole selectivity is lost and the setup behaves similarly to a network of ohmic resistors.

Figure 2(a) shows I_{side} as a function of V_E and V_{BC} [same raw data as Fig. 1(b)]. For $V_E\gtrsim-150$ meV BE is completely closed, hence, current flow is suppressed ($I_{side}=I_C=I_E=0$). As V_E is increased the emitter QPC opens and I_E becomes nonzero. A dashed contour line encloses the region of $I_{side}<0$. The three-dimensional (3D) representation in Fig. 2(b) displays a few contour lines at $I_{side}\leq0$ as a function of V_E and V_{BC} for several emitter configurations V_{BE}. Clearly $I_{side}<0$ only occurs within a narrow tube in a region where the emitter QPC BE is almost pinched off.

The dependence of α on the collector barrier height E_{BC} is also shown in Fig. 2(a) (top axis). E_{BC} can be determined from V_{BC} by measuring the reflection of Landau levels on the barrier in a magnetic field.[12,13] In addition, the calibration point $E_{BC}=E_F$ is known from linear-response transport measurements across the barrier as a function of V_{BC}. A simple one-dimensional (1D) model predicts maximal amplification α_{max} at exactly $E_{BC}=E_F$ since in this case excited electrons would pass BC whereas holes would be reflected. Strikingly, in Fig. 2(a) α_{max} (which almost coincides with I_{side}^{min}) occurs at $E_{BC}<E_F$ ($E_{BC}\simeq E_F-1.4$ meV). This is related to the 2D character of the charge carriers which allows an angle distribution of momenta within the 2DES. A charge carrier can only pass BC if its forward momentum component $p_\perp$ perpendicular to the barrier fulfills $p_\perp^2/2m>E_{BC}$. Compared to the 1D case the barrier has therefore to be lower in 2D for a significant portion of the excited electrons to pass. α_{max} is thus expected at $E_{BC}<E_F$,[14] which is in agreement with experimental data (*angle effect*). In a previous publication, α_{max} at $E_{BC}>E_F$ was reported,[8] though this was obtained with a very different calibration procedure.

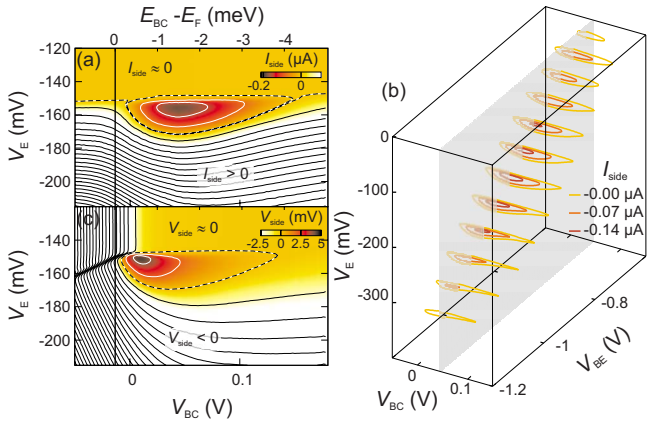

FIG. 2. (Color online) (a) I_{side} as a function of V_E and V_{BC} [same raw data as in Fig. 1(b)]. Contour lines are spaced by 0.07 μA (white for $I_{side}<0$, dashed for $I_{side}\simeq0$). (b) 3D representation of $I_{side}\leq0$ (three contour lines) vs V_E and V_{BC} for several V_{BE}. (c) V_{side} measured at floating side contact, parameters as in Fig. 2(a). Contour lines are spaced by 2 mV (white for $V_{side}>0$, dashed for $V_{side}\simeq0$).

As an alternative to measuring I_{side} in a three-terminal setup, Fig. 2(c) shows V_{side} detected at the floating side contact. In the diffusive regime $V_{side}<0$ would be expected (since $V_E<0$). However, as in the current measurement, scattering of the injected electrons occurs and causes $V_{side}>0$ in a region roughly comparable to that of $I_{side}<0$ in Fig. 2(a). Since this is a two-terminal setup [see sketch in Fig. 1(c)], the continuity equation forces $I_C=I_E$. Electrons cannot escape to the side contact and, hence, the angle effect as described above must be absent. Nevertheless the maximum of $V_{side}>0$ is still observed at $E_{BC}<E_F$. This can be explained by means of a positive charge that builds up between BE and BC in steady state (in a current measurement this charge is at least partly neutralized by $I_{side}<0$). The positive charge causes a decrease in the local chemical potential. Electrons trying to escape via BC thus see a larger *effective* barrier, and hence, the maximum effect is again found at $E_{BC}<E_F$ (*charge effect*).[15]

In Fig. 2(b) a semitransparent plane perpendicular to the cross section of Fig. 2(a) marks constant $V_{BC}=0.045$ V. A detailed measurement of I_{side} within this plane is plotted in

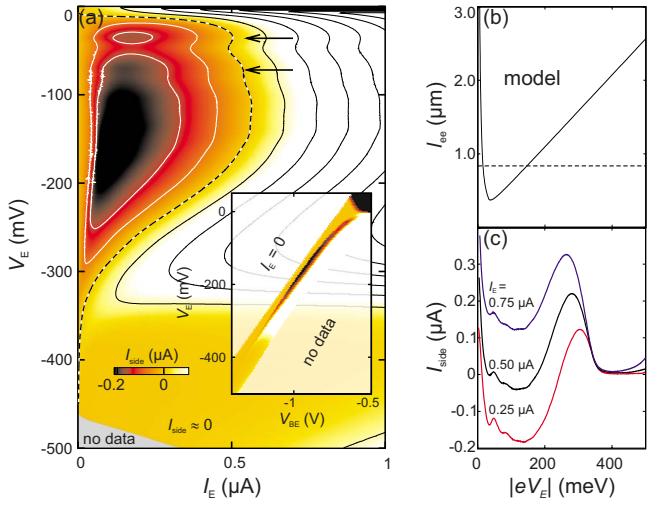

FIG. 3. (Color online) (a) Inset: I_{side} as a function of V_{BE} and V_{E}. No data exist for $V_{\mathrm{E}} \times I_{\mathrm{side}} > 700$ nW and in the upper left region where the emitter QPC is closed and all currents vanish. Main plot: same data as a function of injected current I_{E}. (b) Numerical calculation of the electron-electron scattering length, l_{ee}, as a function of excess kinetic energy $|eV_{\mathrm{E}}| \simeq E_{\mathrm{kin}} - E_{\mathrm{F}}$ at $T=0$. (c) Vertical slices of Fig. 3(a) for three different I_{E}.

the inset of Fig. 3(a). The main plot shows the same I_{side} data as a function of V_{E} and the overall current I_{E}. We observe $I_{\mathrm{side}} < 0$ to the left of the dashed contour line. Figure 3(c) displays vertical cross sections of Fig. 3(a) which show the dependence of I_{side} on the energy of the injected electrons for constant I_{E}. The main behavior seen in Figs. 3(a) and 3(c) is closely related to the electron-electron scattering length l_{ee}. By numerical calculations based on the random-phase approximation, we have extended predictions for the linear-response regime[16,17] to the nonequilibrium case required for our experiments. The calculated l_{ee} is plotted in Fig. 3(b) for $T=0$ as a function of $|eV_{\mathrm{E}}| \simeq E_{\mathrm{kin}} - E_{\mathrm{F}}$, the excess kinetic energy of the injected electrons. As expected, l_{ee} diverges for $E_{\mathrm{kin}} \to E_{\mathrm{F}}$ ($eV_{\mathrm{E}} \to 0$) and then rapidly decreases as E_{kin} is increased.[16,17] At higher E_{kin}, a minimum at $|eV_{\mathrm{E}}| \simeq 5E_{\mathrm{F}}$ is followed by a linear increase in l_{ee} which can be understood in terms of decreasing electron-electron interaction times.

This behavior can be mapped onto the measured energy dependence of I_{side} [Fig. 3(c)] by taking into account the sample geometry [Fig. 1(a)]. The distance between BE and BC is $L_{\mathrm{EC}} \simeq 840$ nm [dashed line in Fig. 3(b)], about twice as long as the minimal calculated l_{ee}. In the extreme limits of $E_{\mathrm{kin}} \to E_{\mathrm{F}}$ or $E_{\mathrm{kin}} \to \infty$, we find $l_{\mathrm{ee}} \gg L_{\mathrm{EC}}$ and expect electrons to move ballistically and without electron-electron scattering within the sample. As the energy is increased starting from $eV_{\mathrm{E}}=0$, l_{ee} decreases, and for $l_{\mathrm{ee}} < L_{\mathrm{EC}}$, a positive charge builds up between BE and BC. It is neutralized by a growing negative component of I_{side} [Fig. 3(c)]. Excited electrons always lose energy when scattering with the cold Fermi sea. Hence, scattering of an excited electron on the negative slope of $l_{\mathrm{ee}}(eV_{\mathrm{E}})$ [Fig. 3(b)] results in carriers with increased l_{ee} for subsequent scattering events. In contrast, scattering of electrons on the positive slope of $l_{\mathrm{ee}}(eV_{\mathrm{E}})$ often results in carriers with decreased l_{ee}. These carriers contribute heavily to a negative I_{side} by multiple scattering events. The measured

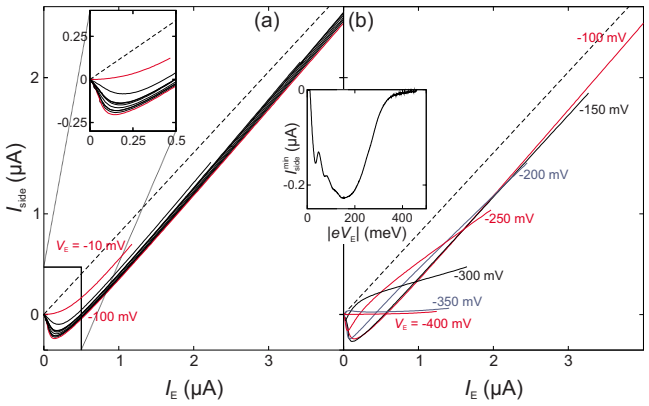

FIG. 4. (Color online) I_{side} as a function of injected current I_{E} for $|V_{\mathrm{E}}| \leq 100$ mV (spacing 10 mV) in (a) and $|V_{\mathrm{E}}| \geq 100$ mV in (b). Dashed straight lines represent ohmic behavior (see main text). The central inset plots $I_{\mathrm{side}}^{\mathrm{min}}$ vs the energy of the injected electrons $|eV_{\mathrm{E}}|$.

$I_{\mathrm{side}}^{\mathrm{min}}(eV_{\mathrm{E}})$ clearly is expected to extend to higher energies compared to the minimum of $l_{\mathrm{ee}}(eV_{\mathrm{E}})$ [Figs. 3(b) and 3(c)]. At larger energies the injected electrons tend to pass BC and scatter beyond the barrier. For l_{ee} only slightly larger than L_{EC}, some of the scattered electrons can travel back across BC and into the side contact, causing the local maximum of $I_{\mathrm{side}}(eV_{\mathrm{E}}) > 0$ visible in Fig. 3(c). For even higher E_{kin} ($eV_{\mathrm{E}} > 350$ mV, $l_{\mathrm{ee}} \gtrsim 3L_{\mathrm{EC}}$) we find an extended regime with $I_{\mathrm{side}} \simeq 0$ ($I_{\mathrm{C}} \simeq I_{\mathrm{E}} > 0$). Here l_{ee} exceeds the sample dimensions by far so that electron-electron scattering happens far beyond BC and all resulting charge carriers end up in the grounded collector contact C. This behavior ($I_{\mathrm{side}} \simeq 0$) emphasizes the ballistic nature of the hot electrons in our experiments which goes beyond previously published results.[3–5]

Cross sections of Fig. 3(a) at constant excess kinetic energy $|eV_{\mathrm{E}}|$ allow us to discuss the dependence of I_{side} on the total current I_{E} and are displayed as line plots for $|V_{\mathrm{E}}| \leq 100$ mV in Fig. 4(a) and for $|V_{\mathrm{E}}| \geq 100$ mV in Fig. 4(b). The dashed straight lines represent the expectation for ohmic behavior ($I_{\mathrm{side}} \propto I_{\mathrm{E}}$) with a slope determined by measuring the two-terminal resistances of the device in the linear-response regime. For $I_{\mathrm{E}} \gtrsim 0.3$ μA and within the broad minimum of $I_{\mathrm{side}}(eV_{\mathrm{E}})$ seen in Fig. 3(c) (40 meV $\lesssim |V_{\mathrm{E}}| \lesssim$ 150 mV), all curves coincide and are almost parallel to the ohmic line. This behavior is plausible for small enough l_{ee} when multiple scattering events and reflections, e.g., at BC, scramble the electrons. Under these conditions the initial momentum of the injected electrons becomes less important for the direction of current. However, in our case ohmic behavior is superimposed with a ballistic effect, a negative contribution to I_{side} due to the separation of electrons and holes at BC.

As I_{E} is increased from $I_{\mathrm{E}}=0$ by adjusting V_{BE}, more and more electron-hole pairs are created and partly separated at BC. Only part of the positive charge of the holes can be neutralized from the side contact due to its finite resistance. The remaining positive charges lower the chemical potential of the Fermi sea between BE and BC (charge effect) so that less excited electrons escape via BC. The reflected electrons cause additional neutralization of holes. The neutralization rate therefore increases with increased I_{E}, and the steady-

state negative component of I_{side}, reached when hole creation and neutralization rates balance, saturates for large I_E. For higher energies and longer l_{ee}, deviations from this behavior occur as the injected electrons move forward ballistically [Fig. 4(b)].

The central inset in Fig. 4 displays I_{side}^{min} as a function of the energy $|eV_E|$ of the injected electrons. Similar to Fig. 3(c) it once again states the strong energy dependence of the amplification effect already discussed above. The local minima at $|eV_E| \simeq 36$ meV and 72 meV are caused by emission of optical phonons.[7,10] They can also be seen in Fig. 3(c) and more distinct in Fig. 3(a) (two black arrows at $V_E = 36$ and 72 meV).

Finally, it is important to differentiate the observed electronic Venturi effect from a thermoelectric effect caused by Joule heating. Such thermal effects are usually described within local equilibrium in the diffusive regime and mainly depend on the dissipated power. Figure 4 can be used to analyze I_{side} as a function of power $P = |V_E I_E|$ since V_E is constant for each curve. The negative contribution to I_{side} saturates as P is increased, whereas in a thermoelectric effect it would be expected to grow further. The amplification ratios for thermally driven effects are also expected to be much smaller[4] compared to the α we find, which again confirms the role of ballistic motion for the observed effects. In addition, the strong dependence of α on the energy of the injected electrons [Fig. 3(a)], as well as the maximum α occurring for $E_{BC} < E_F$ [Fig. 2(a)], are in direct contradiction to an interpretation in terms of a thermoelectric effect.

As a result, we have built a prototype of an electron-avalanche amplifier. It is based on a jet pump explained by the electronic Venturi effect, namely, scattering of hot electrons with a degenerate Fermi liquid. Our systematic investigations go well beyond earlier publications and provide a comprehensive picture of the physics involved in the ballistic nonequilibrium regime. We present a consistent model based on electron-electron scattering and electron-hole neutralization which agrees qualitatively with our experimental results. Modifications in geometry and circuitry will result in improved electron jet pumps with potential applications, e.g., as a noninvasive charge detector. In such a device a single electron originating from a quantum dot would trigger a current pulse strong enough to be detected.

We thank J. P. Kotthaus, A. Govorov, L. Molenkamp, M. Heiblum, I. Kaya, and F. Marquardt for fruitful discussions. Financial support by the German Science Foundation via SFB 631, SFB 689, LU 819/4-1, and the German Israel program DIP, the German Excellence Initiative via the "Nanosystems Initiative Munich (NIM)," and LMUinnovativ (FuNS) is gratefully acknowledged.

[1] A. O. Govorov and J. J. Heremans, Phys. Rev. Lett. **92**, 026803 (2004).
[2] R. Bunsen, Philos. Mag. Ser. 4 **37**, 1 (1869).
[3] M. Heiblum, Solid-State Electron. **24**, 343 (1981).
[4] B. Brill and M. Heiblum, Phys. Rev. B **49**, 14762 (1994).
[5] I. I. Kaya *et al.*, Semicond. Sci. Technol. **11**, L135 (1996).
[6] A. Palevski, C. P. Umbach, and M. Heiblum, Appl. Phys. Lett. **55**, 1421 (1989).
[7] U. Sivan, M. Heiblum, and C. P. Umbach, Phys. Rev. Lett. **63**, 992 (1989).
[8] I. I. Kaya and K. Eberl, Phys. Rev. Lett. **98**, 186801 (2007).
[9] G. J. Schinner, H. P. Tranitz, W. Wegscheider, J. P. Kotthaus, and S. Ludwig, Phys. Rev. Lett. **102**, 186801 (2009).
[10] A. S. Dzurak, C. J. B. Ford, M. J. Kelly, M. Pepper, J. E. F. Frost, D. A. Ritchie, G. A. C. Jones, H. Ahmed, and D. G. Hasko, Phys. Rev. B **45**, 6309 (1992).
[11] H. Predel, H. Buhmann, L. W. Molenkamp, R. N. Gurzhi, A. N. Kalinenko, A. I. Kopeliovich, and A. V. Yanovsky, Phys. Rev. B **62**, 2057 (2000).
[12] S. Komiyama, H. Hirai, S. Sasa, and S. Hiyamizu, Phys. Rev. B **40**, 12566 (1989).
[13] R. J. Haug, A. H. MacDonald, P. Streda, and K. von Klitzing, Phys. Rev. Lett. **61**, 2797 (1988).
[14] Simple estimations agree well with the observed magnitude of the angle effect.
[15] In the regime where BE and BC are closed [top left corner of Fig. 2(c)], the side contact is electrically insulated. Here the potential V_{side} is frozen at a constant value depending on the experimental history [in Fig. 2(c) we have performed vertical sweeps].
[16] A. V. Chaplik, Zh. Eksp. Teor. Fiz. **60**, 1845 (1971).
[17] G. F. Giuliani and J. J. Quinn, Phys. Rev. B **26**, 4421 (1982).